Quantifying the Strength and Delay of Climatic Interactions: The Ambiguities of Cross Correlation and a Novel Measure Based on Graphical Models

JAKOB RUNGE

Potsdam Institute for Climate Impact Research, Potsdam, and Department of Physics, Humboldt University, Berlin, Germany

VLADIMIR PETOUKHOV

Potsdam Institute for Climate Impact Research, Potsdam, Germany

JÜRGEN KURTHS

Potsdam Institute for Climate Impact Research, Potsdam, and Department of Physics, Humboldt University, Berlin, Germany, and Institute for Complex Systems and Mathematical Biology, University of Aberdeen, Aberdeen, United Kingdom

(Manuscript received 12 March 2013, in final form 5 September 2013)

ABSTRACT

Lagged cross-correlation and regression analysis are commonly used to gain insights into interaction mechanisms between climatological processes, in particular to assess time delays and to quantify the strength of a mechanism. Exemplified on temperature anomalies in Europe and the tropical Pacific and Atlantic, the authors study lagged correlation and regressions analytically for a simple model system. A strong dependence on the influence of serial dependencies or autocorrelation is demonstrated, which can lead to misleading conclusions about time delays and also obscures a quantification of the interaction mechanism.

To overcome these possible artifacts, the authors propose a two-step procedure based on the concept of graphical models recently introduced to climate research. In the first step, graphical models are used to detect the existence of (Granger) causal interactions that determine the time delays of a mechanism. In the second step, a certain partial correlation and a regression measure are introduced that allow one to specifically quantify the strength of an interaction mechanism in a well interpretable way that enables the exclusion of misleading effects of serial correlation as well as more general dependencies. The potential of the approach to quantify interactions between two and more processes is demonstrated by investigating teleconnections of ENSO and the mechanism of the Walker circulation.

The article is intended to serve as a guideline to interpret lagged correlations and regressions in the presence of autocorrelation and introduces a powerful approach to analyze time delays and the strength of an interaction mechanism.

1. Introduction

Lagged correlation analysis is a simple and very common method in many fields of science, popularized in climate research already by the seminal works of Walker (1923, 1924). It is a first step to gain insights into the possible interaction mechanisms between different processes. Specifically, the cross-correlation lag function is used to assess the time delay and to quantify the strength of the link mediated by a certain mechanism. To name just a few examples, Lanzante (1996) computed lag correlations of sea surface temperatures between different tropical regions to assess their mutual interaction. Klein et al. (1999) studied the mechanism by which the El Niño–Southern Oscillation (ENSO) influences the Atlantic and Indian Oceans and southern China. They inferred time delays between 3 and 6 months and suggest that changes in atmospheric circulation accompanying El Niño induce changes in cloud cover and evaporation that, in turn, increase the net heat flux entering these remote oceans. This was then postulated to be responsible for the surface warming. Gu and Adler (2011) investigated the impact of ENSO on tropical land surface temperatures

Corresponding author address: Jakob Runge, Potsdam Institute for Climate Impact Research (PIK), Telegraphenberg A 31, 14473 Potsdam, Germany.
E-mail: jakobrunge@gmail.com

DOI: 10.1175/JCLI-D-13-00159.1

and precipitation and find that the influence of ENSO on land precipitation has much shorter lags than the effect on land temperatures. They interpret this difference by suggesting, ''This 5-month time lag suggests a rough time scale needed for land surface air temperature to adjust because of the variations of surface energy budget caused by ENSO-associated circulation and precipitation anomalies.'' Hashizume et al. (2009) inferred a more complicated mechanism by investigating the impact of the Indian Ocean dipole (DMI) on the malaria risk in western Kenya. They find that ''the 3- to 4-month lag in the positive association between DMI and the number of malaria cases coincided with the sum of the lag between DMI and rainfall (1 month) and the lag between rainfall and the incidence of malaria (2–3 months).''

These examples demonstrate that the cross correlation's maximum delay is used in interpreting the delay of the underlying physical mechanism that couples two processes. Apart from the analysis of time lags, the value of the cross correlation is commonly used as a measure of the effect of one process on another or a measure of the strength of a link or association, in line with the statistical interpretation of the square of correlation as the proportion of variance of one process that can be linearly represented by the other (Von Storch and Zwiers 2002; Chatfield 2003). These analyses are often accompanied by regressions.

But is it really justified to infer physical time lags from the maximum of the cross-correlation function? How reliable is this method? The delay of what mechanism is actually measured? And how can the value of the cross correlation be interpreted *physically*?

Through a motivating example in the next section, we will show that these conclusions about a physical mechanism are strongly dependent on many factors. Generally, often climatological time series exhibit serial correlations or serial dependencies, often also referred to as autocorrelations or time series featuring a red noise spectrum (Von Storch and Zwiers 2002). Especially in tropical temperature time series, where the temperature at a given month very much depends on the temperatures of the previous months. In this article, the influence of serial correlation on lagged correlation functions and regressions will be in detail analytically investigated on a simple linear model system. It will be demonstrated how this influence can lead to misleading conclusions about time delays and how it also obscures a quantification of the interaction mechanism and, therefore, misguides a physical interpretation.

To overcome these possible artifacts, we propose a two-step procedure based on the concept of *graphical models* that has recently been introduced to climate research (Ebert-Uphoff and Deng 2012a). In a first step, the framework of graphical models is used to detect the existence of (Granger) causal interactions yielding the interaction time delays, while in a second step a certain partial correlation and a regression measure are introduced that allow one to specifically quantify the strength of an interaction mechanism in a well interpretable way. We will demonstrate that our approach goes beyond the pure graphical models analysis of Ebert-Uphoff and Deng (2012a) and enables us to exclude the misleading effects of serial correlation as well as more general external dependencies. Our method is then applied to tropical and European midlatitude time series with strong and weak autocorrelations to demonstrate the different effects on an assessment of a coupling mechanism. As a further step, the potential of the approach to quantify the interactions also between more than two variables is demonstrated to shed light on the mechanism of the Walker circulation. The classical correlation and the novel partial-correlation approach are discussed regarding their statistical as well as their climatological implications.

The article is structured as follows: In section 2, a motivating example from two very different pairs of time series data is given, and section 3 gives detailed analytical derivations for the cross correlation and regressions of a typical simple model example. In the light of the studied examples, the physical interpretation of correlations and regressions is discussed in section 4. As a solution to the problem, in section 5 the framework of graphical models and its relation to the concept of Granger causality is introduced and in section 6 the proposed partial correlation and regression measures will be defined and some important characteristics discussed. Finally, in section 7 several teleconnection examples and the Walker circulation are analyzed. The climatological implications are discussed in section 8. We focus on climatological examples in the main text and provide further theoretical results and discussions in the appendixes.

2. Motivating example

To motivate the problem considered here, cross-correlation and autocorrelation functions for two very different pairs of monthly surface temperature anomalies from the NCEP–NCAR reanalysis (Kalnay et al. 1996) are analyzed for the period 1948–2012 with 780 months. Anomalies are taken with respect to the whole period. In the first example, Niño-3 is the time series of the spatial average over the Niño-3 region in the eastern Pacific and ATL is the average over a region in the tropical North Atlantic (all regions are shown on the map in Fig. 10). In the second example, the cross correlation between two time series from Europe is studied. WEUR is the average over a region in western Europe

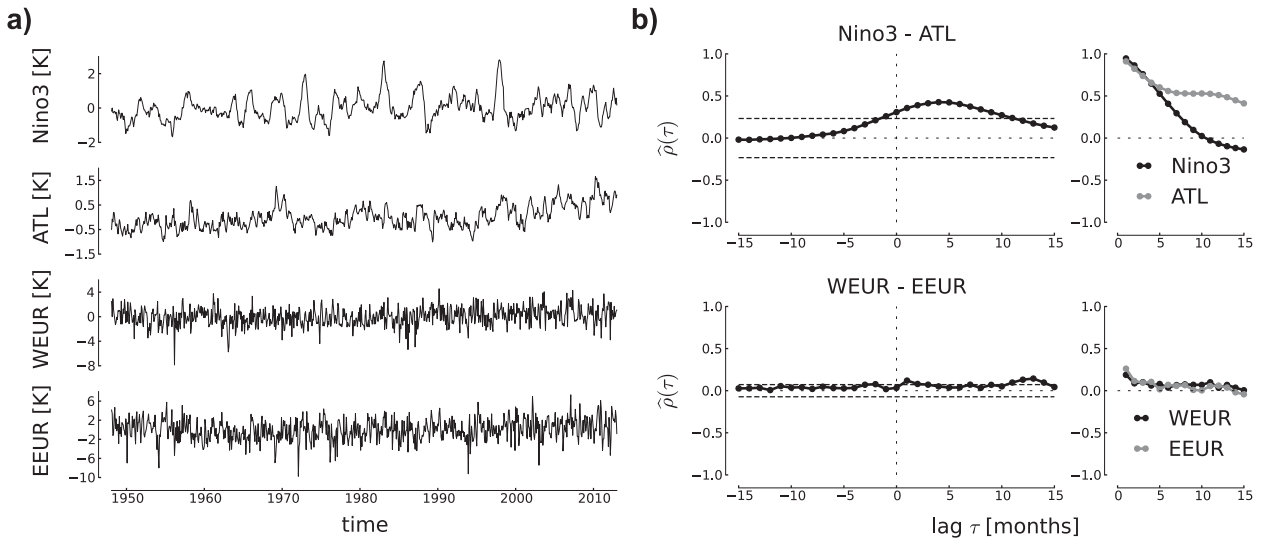

FIG. 1. (a) Time series and (b) estimated (left) cross-correlation and (right) autocorrelation functions for monthly temperature anomalies from the Niño-3, ATL, WEUR, and EEUR regions. All regions are shown on the map in Fig. 10. The lag-1 autocorrelation coefficients are 0.95 (Niño-3), 0.91 (ATL), 0.19 (WEUR), and 0.26 (EEUR). In (b), the two-tailed $\alpha = 95\%$ significance threshold (dashed) for cross correlation is computed from uncorrelated Gaussian surrogate time series with the same autocorrelation coefficients and variances as the data. Note that for the autocorrelations the 0 lag is not shown. The plots demonstrate apparent differences in the cross correlations that can be attributed to much stronger persistence in the tropical time series.

at 45°–55°N, 0°–10°E, and EEUR is the average over a region in eastern Europe at 45°–55°N, 40°–50°E. Figure 1a shows the time series and Fig. 1b shows the cross-correlation and autocorrelation functions.

Several observations are apparent from Fig. 1b: the peak of the tropical cross correlation with its maximum $\hat{\rho} = 0.43$ at lag +4 is higher and broader than those of the European cross correlation that has values above the significance threshold only at lag +1 ($\hat{\rho} = 0.12$) and from around +12 to +13 months ($\hat{\rho} = 0.13 - 0.14$). A correlation between the eastern Pacific and the tropical Atlantic is also reported in Lanzante (1996), where a lag of around 6 months with a correlation of 0.34 was found.

Interpreting cross correlation as a measure of the strength of a link mediated via a climatic mechanism, we have to ask, do these results imply that the Pacific–Atlantic link over a distance of about 4500–8500 km (depending on whether the region's corners or centers are used) is stronger than the link in Europe with a distance of only 2000–3000 km? Can one infer that the mechanism in the tropics is present at the whole range of lags from −1 to +11 months, since these lags are significantly correlated? Does the mechanism to transfer the Pacific anomalies take 4 months to reach the Atlantic? Note that the significance test used here assumes two uncorrelated Gaussian lag-1 autoregressive [AR(1)] processes and thus accounts for autocorrelation. We also estimated univariate regressions as shown in Table 1 that also give a larger coefficient for the tropical interaction.

One explanation for the differences between the tropical and European correlations could be the much stronger persistence, that is, autocorrelation in the tropical time series as can be seen from the slowly decaying autocorrelation functions Fig. 1b. The autoregressive lag-1 coefficients are 0.95 (Niño-3) and 0.91 (ATL), but only 0.19 (WEUR) and 0.26 (EEUR). These differences seem to very much affect the cross-correlation lag function, which raises the question how in particular a peak value and the lag at which the maximum occurs are to be interpreted. This question will be addressed in the next section and some geophysical explanations will be given in section 4.

3. Correlation and regression of model example

To investigate how the value and lag at the maximum of the cross-correlation function and regression coefficients depend on serial correlation, consider the following bivariate first-order autoregressive process of two serially correlated subprocesses with a unidirectional influence of X on Y:

TABLE 1. Results of univariate regression analyses of time series in the tropics and Europe (after subtracting their mean).

Dependent Variable	Coef (lag τ)	Estimate	Std error	p value
ATL	Niño-3 (4)	0.27	0.02	$<10^{-5}$
EEUR	WEUR (1)	0.18	0.05	≈ 0.001

TABLE 2. Analytical comparison of lagged cross-correlation and the partial-correlation measures ITY and MIT as well as univariate and multivariate MIT regressions for the model example Eq. (1) on the dependent variable Y. The parents used in ITY and MIT for this model are $\mathcal{P}_{Y_t} = \{Y_{t-1}, X_{t-1}\}$ and $\mathcal{P}_{X_t} = \{X_{t-1}\}$. For the contemporaneous link $X_t - Y_t$, the MIT regression coefficient $B_{(X_{\mathcal{P}_X})_t}$ corresponds to the quotient of the residual's covariance and variance after lagged MIT regressions of X on its parents yielding $B_{X_{t-1}} = a$ and Y on its parents yielding $(B_{X_{t-1}}, B_{Y_{t-1}}) = (c, b)$. The formulas demonstrate the dependence of cross-correlation and univariate regressions on the autocorrelations strengths a and b. Interestingly, for this model ITY still depends on the autocorrelation strength of Y, while MIT fully excludes both autocorrelation influences.

Model example Eq. (1) for $\sigma_{XY} = 0$	Model example Eq. (1) for $\sigma_{XY} = 0$	Eq. (1) for $c = 0$
cross correlation $\rho(X_{t-\tau}; Y_t)$	univariate regression	univariate regression
$= \begin{cases} \dfrac{a^{1+\lvert\tau\rvert} c\sigma_X^2}{(1-a^2)(1-ab)} \Big/ \sqrt{\Gamma_X \Gamma_Y} & \text{for} \quad \tau \le 0 \\ \dfrac{c\sigma_X^2 [a^{\lvert\tau\rvert}(1-ab) - b^{\lvert\tau\rvert}(1-a^2)]}{(1-a^2)(a-b)(1-ab)} \Big/ \sqrt{\Gamma_X \Gamma_Y} & \text{for} \quad \tau > 0 \end{cases}$	$B_{X_{t-1}} = \dfrac{c}{1-ab}$	$B_{X_t} = \dfrac{(1-a^2)\sigma_{XY}}{(1-ab)\sigma_X^2}$
with $\Gamma_X = \dfrac{\sigma_X^2}{1-a^2}$, $\Gamma_Y = \dfrac{c^2\sigma_X^2(1+ab) + \sigma_Y^2(1-a^2)(1-ab)}{(1-a^2)(1-b^2)(1-ab)}$		
partial correlation $\rho^{\mathrm{ITY}}_{X \to Y}(\tau)$		
$= \begin{cases} \sqrt{\dfrac{c^2\sigma_X^2[c^2\sigma_X^2 + (1-ab)^2\sigma_Y^2]}{c^4\sigma_X^4 + 2(1-ab)c^2\sigma_X^2\sigma_Y^2 + (1-a^2)(1-ab)^2\sigma_Y^4}} & \text{for} \quad \tau = 1 \\ 0 & \text{for} \quad \tau \ne 1 \end{cases}$		
partial correlation $\rho^{\mathrm{MIT}}_{X \to Y}(\tau)$	MIT regression	MIT regression
$= \begin{cases} \dfrac{c\sigma_X}{\sqrt{c^2\sigma_X^2 + \sigma_Y^2}} & \text{for} \quad \tau = 1 \\ 0 & \text{for} \quad \tau \ne 1 \end{cases}$	$\mathbf{B}_{\mathcal{P}_{Y_t}} = \begin{pmatrix} B_{X_{t-1}} \\ B_{Y_{t-1}} \end{pmatrix} = \begin{pmatrix} c \\ b \end{pmatrix}$	$B_{(X_{\mathcal{P}_X})_t} = \dfrac{\sigma_{XY}}{\sigma_X^2}$

$$X_t = aX_{t-1} + \varepsilon_t^X$$
$$Y_t = bY_{t-1} + cX_{t-1} + \varepsilon_t^Y, \qquad (1)$$

where $(\varepsilon^X, \varepsilon^Y)$ are independent and identically distributed Gaussian random variables, sometimes referred to as the *innovations,* with zero mean and covariance matrix

$$\mathbf{\Sigma} = \begin{pmatrix} \sigma_X^2 & \sigma_{XY} \\ \sigma_{XY} & \sigma_Y^2 \end{pmatrix}. \qquad (2)$$

In the following, a and b—commonly regarded as the persistence of a process—are assumed positive as is often the case for climate time series (Von Storch and Zwiers 2002).

a. Cross-correlation lag function

The cumbersome formula of the lagged cross correlation can be found in Table 2 in a comparison with the novel introduced partial-correlation measures. Already from this formula we see that the correlation function $\rho_{YX}(\tau)$ clearly not only depends on c and the variances, but also on the autocorrelation coefficients a and b. To illustrate this dependence, we show in Figs. 2a and 2b plots of $\rho_{YX}(\tau)$ for fixed coupling coefficient $c = 0.1$ and different autoregressive coefficients a while keeping $b = 0.9$ fixed in Fig. 2a and vice versa in Fig. 2b.

Several observations can be made. The height of the peak of the correlation function for the same small coupling coefficient $c = 0.1$ strongly varies from very low to very high values for increasing autocorrelation strength a (Fig. 2a). Especially for large autocorrelation even a slight variation in a of 0.025 causes an increase in ρ of about 0.1. On the other hand, for increasing b the maximum first increases and for very large b decreases again (Fig. 2b) with an overall variation in ρ of about 0.3. Also, the lag at which the maximum occurs is shifted toward larger lags for increasing a and b. This can happen even for low autocorrelations like $b = 0.6$ and $a = 0.7$, while for tropical temperature anomalies values above 0.9 are very common as is the case in our motivating example. Also here, for high autocorrelations, even for a slight variation in b of 0.025, the maximum's lag is shifted by up to 4 lags. In Figs. 2c and 2d, the value and lag of the maximum are plotted for all combinations of a and b. The maximum's value and lag are rather asymmetric and strongly nonlinear in their dependence on the coefficients. For increasing a the maximum can easily become very large and for additional large b the lag can be strongly shifted.

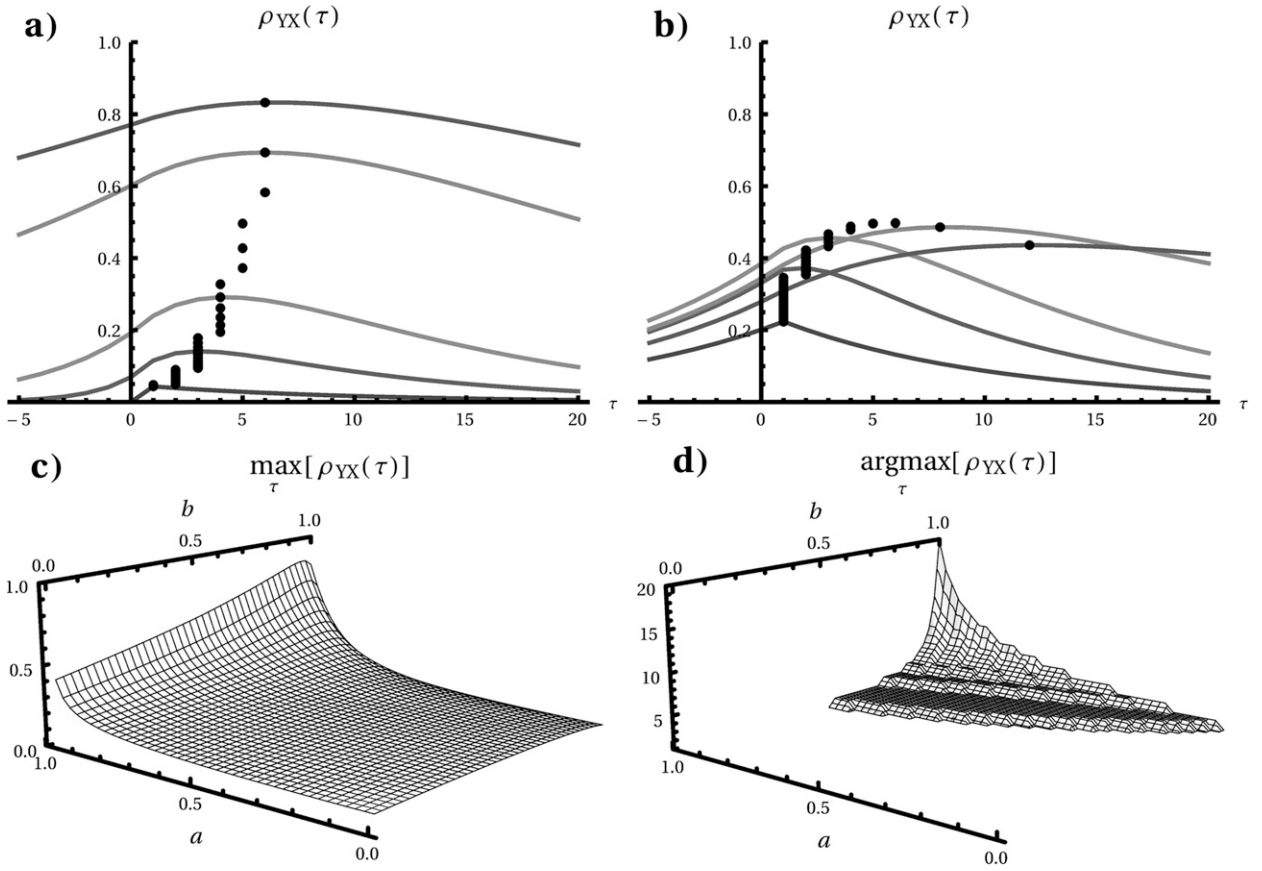

FIG. 2. Plots of the analytical cross-correlation function given in Table 2 for model Eq. (1). (a) The correlation function for fixed $c = 0.1$, $\sigma_X = \sigma_Y = 1$, zero contemporaneous dependence $\sigma_{XY} = 0$, $b = 0.9$, and varying $a = 0$, 0.6, 0.8, 0.95, and 0.975 (bottom to top). The black dots indicate the maxima for the whole range from $a = 0$ to $a = 0.975$ in steps of 0.025. (b) The reverse case where $a = 0.9$ is fixed and b varies in the same range. (c) The value of the maximum and (d) the maximum's lag for varying a and b. In (d), only the region where the lag is shifted is plotted. In the model—assuming zero contemporaneous dependence $\sigma_{XY} = 0$—, this region is independent of c and given by $b > 1/2$ and $a > (1 - b)/b$ assuming positive a and b. Note that the a axis has been reversed for better visibility. The plots demonstrate the strong and nonlinear dependence of the correlation function on the autoregressive coefficients.

In Fig. 3 a case with additional contemporaneous covariance $\sigma_{XY} = 0.6$ is shown. Especially for the two upper curves, albeit the maximum is at lag 0, one is still tempted to interpret the larger correlation for negative lags as a sign for a mechanism where Y drives X, while actually the opposite is the case. Note that often interactions appear contemporaneous due to a low time resolution of the data, which can cause misleading physical interpretations.

b. Regressions

It is a common approach in regression analysis to regress Y on X at the lag with maximum correlation. As studied in the previous paragraph, this can yield very misleading lags. Here, two cases are studied: (i) where the directional coupling coefficient is set $c = 0$, but the contemporaneous dependence σ_{XY} is nonzero (then the maximum is at lag 0); and (ii) with the contemporaneous covariance coefficient set to $\sigma_{XY} = 0$. Then, for moderately strong autocorrelation coefficients in model Eq. (1), that is, outside the region shown in Fig. 2d, the maximum will be at lag 1. For both cases the regression of Y_t on X_t and X_{t-1}, respectively, the coefficients B_{X_t} and $B_{X_{t-1}}$ can easily be derived from the covariances (given in appendix B) demonstrating their dependence on a and b. The formulas are again shown in Table 2 for comparison. In Fig. 4 the quotients of these coefficients divided by the coefficients B'_{X_t} and $B'_{X_{t-1}}$ for zero a and b are plotted for varying a and b to illustrate the factor by which the regression coefficient is changed because of autocorrelation. The plots show that the regression coefficient for contemporaneous regressors can become zero (in the limit $a \to 1$) or even twice as large depending on a and b (Fig. 4a), while for lagged regressors it varies nonlinearly in a and b and

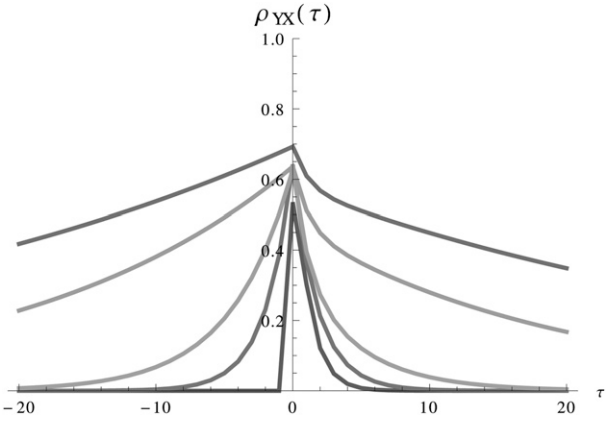

FIG. 3. Plot of the analytical cross-correlation function for model Eq. (1) for fixed $c = 0.1$, $\sigma_X = \sigma_Y = 1$, contemporaneous dependence $\sigma_{XY} = 0.6$, $b = 0.4$, and varying $a = 0, 0.6, 0.8, 0.95$, and 0.975 (bottom–top). The plot shows that autocorrelation could even lead to a misinterpretation of the direction of influence.

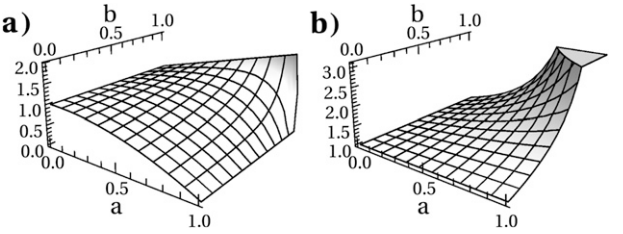

FIG. 4. (a) Plots of quotients $B_{X_t}/B'_{X_t} = (1 - a^2)/(1 - ab)$ for a contemporaneous regression [case (i)] and (b) $B_{X_{t-1}}/B'_{X_{t-1}} = 1/(1 - ab)$ for a lagged regression [case (ii)]. These quotients describe the factor by which the regression coefficients are altered due to autocorrelations a and b. Note that the quotient $B_{X_{t-1}}/B'_{X_{t-1}}$ goes to infinity for $a = b = 1$. The plots demonstrate the strong nonlinear dependence of univariate regressions on autocorrelation.

can be larger by orders of magnitude due to autocorrelation (Fig. 4b). Interestingly, for zero autocorrelation $a = 0$ in X, the autocorrelation b in Y makes no difference.

Summarizing, both the maximum's value and lag of the lagged cross correlation as well as regression coefficients are strongly affected by large autocorrelations and cannot be easily related to the coefficients of the underlying model. For high autocorrelations, these commonly applied measures are, therefore, not even a good first-order approximation of the lag and coupling coefficient of the underlying model. In the next section, we provide a physical picture for this effect and discuss its implications.

4. Geophysical interpretation and discussion

There are also observational examples that agree with our analytical findings. To name just two, in the example from Gu and Adler (2011) mentioned in the introduction, ENSO was found to influence land precipitation with much shorter lags compared to land temperatures (their Figs. 4c,d). In light of our analysis this finding can be interpreted differently: the coupling delay of the mechanism of ENSO's influence on temperature and precipitation might be the same and just the precipitation has a much lower autocorrelation as often is the case for precipitation data. Also, in Huang et al. (2011) the correlations of meteorological variables on malaria are found to be much weaker after *prewhitening* the time series. Prewhitening refers to the procedure to fit and remove an AR(1) model from the time series that obviously decreases serial correlation.

How can these results be interpreted physically? And what do these results mean for the interpretability of correlation as a measure of the delay and link strength of a mechanism? To give a physical intuition, Eq. (1) for $\sigma_{XY} = 0$ can be interpreted as a model of two particles fluctuating around an equilibrium state in their parabolic potential wells (i.e., two Ornstein–Uhlenbeck processes). As visualized in Fig. 5, a strong autocorrelation in Y (large b) can then be understood as a very shallow potential well that leads to the particle taking large departures from its equilibrium position before slowly coming back, giving rise to a strong persistence in the time series. A shallow potential well also renders the particle Y more susceptible to external fluctuations. If also the particle X is immersed in a shallow potential well, a more persistent external force is exerted on Y. Thus, for large autocorrelations these two effects act together leading to a large covariation of X and Y slowly decaying back to their equilibrium, which implies that even if the coupling strength c is small, X has a large effect on Y, and consequently there is a larger cross correlation. Further, for increasing b the delay is shifted toward larger lags due to the strong inertia of Y. But where does the ''shallow

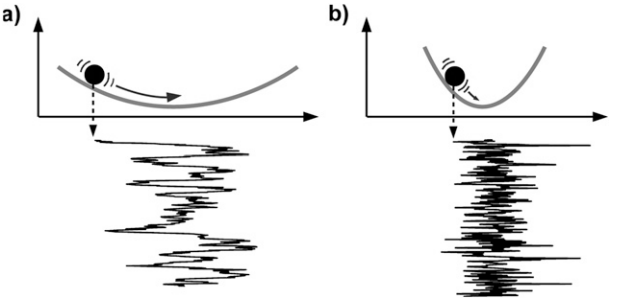

FIG. 5. Physical picture of persistence or autocorrelation via a model of a particle in a potential well subject to stochastic forcing: (a) a shallow potential well leading to large autocorrelation and (b) a narrower well leading to a weaker autocorrelation.

potential well'' come from in the example of surface temperatures in the tropics, and where does the ''narrower potential well'' come from in Europe? Geophysically, one reason for more inertia in the tropical surface temperatures above the ocean is the higher specific heat capacity of the ocean leading to dampened temperature fluctuations. Accordingly, the almost vanishing autocorrelation for the European time series can be well explained by the ''short-term memory'' of the midlatitude atmosphere. More climatological interpretations will be given in comparison with the novel measures in section 8.

The important point now is that only the coefficient c reflects the actual factor of the mechanism by which X influences Y. And since this factor is still dependent on the units of the variables, only c normalized by the innovation's variances reflects the actual strength of the mechanism. Further, only the lag occurring in the physical equation reflects the actual delay (e.g., in delay differential equations). Then, again, we stress that the analysis implies that the cross correlation is not even a good first-order approximation of the coupling strength, and the maximum's lag is also not a good indicator of the coupling delay of the mechanism. Rather, the analysis demonstrates their strong sensitivity even on slight deviations in high autocorrelation. But should a measure of coupling strength and delay between X and Y depend on their internal dynamics, here given by the width of their potentials?

In many statistical methods the effect of autocorrelation is not desired and these methods are, therefore, modified to account for autocorrelation, for example, in the context of trend estimation (Zhang 2004) and the detection of regime shifts (Rodionov 2006) or changepoints (Wang 2008). Also, one usually accounts for autocorrelation in assessing the significance of a cross correlation (e.g., via permutation tests; Zwiers 1990; Ebisuzaki 1997) because autocorrelation inflates the sample cross-correlation coefficient even for independent time series. Further, it is known that for autocorrelated data the significance tests of adjacent lags in the cross-correlation lag function are not independent anymore (Von Storch and Zwiers 2002). Apart from the linear framework studied here, the qualitative properties for the cross correlation also hold for the lag function of the more general information–theoretic mutual information (Cover and Thomas 2006) since it does not take into account autocorrelation. Mutual information and more measures are in detail studied in Runge et al. (2012a).

Now we propose to also account for autocorrelation and even more general ''external'' dependencies in assessing the strength and lag of a mechanism to avoid the problems analyzed in the previous sections. To be clear, this does not refer to problems of the estimate of the cross-correlation coefficient but to the theoretical properties of the cross-correlation function. Our solution developed in the next sections is based on the framework of graphical models, in which we derive a partial-correlation measure that is not as ambiguous and is better interpretable than cross correlation as demonstrated analytically and on climatic examples.

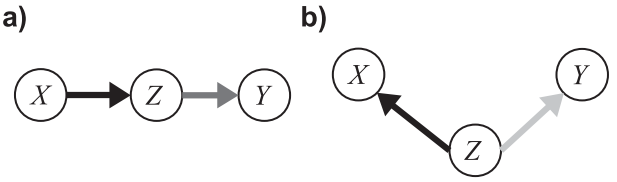

FIG. 6. Causality between three processes: (a) indirect chain and (b) common driver system. The shading of links underlines the difference between the graphical models approach that only assesses the existence of causal links and our approach to additionally quantify their strength.

5. Graphical models and causality

The application of graphical models (Lauritzen 1996) in climate research was recently suggested by Ebert-Uphoff and Deng (2012a,b) who also provide a thorough overview of the concept. Therefore, the introduction is kept brief here. Graphical models provide a tool to distinguish direct from indirect interactions between and within multiple processes. Underlying is the concept of *conditional independencies* in a general multivariate process, which can be explained as follows. Consider three processes where X drives Z and Z drives Y as visualized in Fig. 6a. Here, X and Y are not directly but indirectly interacting and in a bivariate analysis X and Y would be found to be dependent—implying that their correlation would be nonzero in the case of a linear dependency. The same holds for a common driver scheme in Fig. 6b. In larger systems there are usually many more indirect connections than direct ones, and a bivariate analysis would show many nonzero correlations without containing much actual information about the underlying causality.

If, however, the variable Z is included into the analysis, one finds that X and Y are independent *conditional* on Z, written as

$$X \perp\!\!\!\perp Y \,|\, Z.$$

This implies that the joint probability density $p(X, Y, Z)$ factorizes into a product of conditional probability densities.

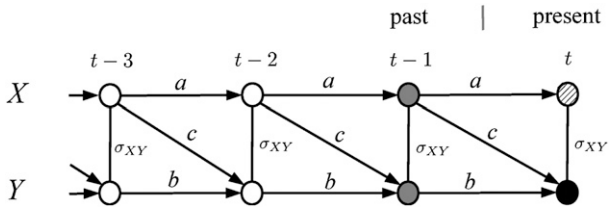

FIG. 7. Visualization of model Eqs. (5) and (1) as a time series graph. Each node corresponds to a lagged subprocess and owing to stationarity links for t imply links for all $t-1, t-2, \ldots$. Process Y_t (black node) has two parents (gray nodes, connected via incoming links from the past) and one neighbor X_t (hatched node, connected with an undirected contemporaneous link) as defined in Eqs. (6) and (7). In the case of a linear model, each multivariate regression coefficient a, b, and c can be attributed to a link.

a. Definition of time series graphs

Time series graphs are based on the concept of conditional independence like graphical models and were introduced for the linear case by Dahlhaus (2000) and Eichler (2005, 2012) and in a certain nonlinear generalization to phase synchronization (Schelter et al. 2006). As depicted in Fig. 7 for model Eq. (1), each node in that graph represents a single random variable (i.e., a subprocess of a multivariate process $\mathbf{X}$) at a certain time t. Compared to the general concept of graphical models that is applicable also to data without time ordering, for time series graphs the time dependence is explicitly used to define directional links. Nodes $X_{t-\tau}$ and Y_t are connected by a directed link $X_{t-\tau} \to Y_t$ pointing forward in time if and only if $\tau > 0$ and

$$X_{t-\tau} \not\perp\!\!\!\perp Y_t \,|\, \mathbf{X}_t^- \backslash \{X_{t-\tau}\}, \tag{3}$$

that is, if they are *not* independent conditionally on the past of the whole process denoted by $\mathbf{X}_t^- = (\mathbf{X}_{t-1}, \mathbf{X}_{t-2}, \ldots)$ excluding $X_{t-\tau}$ (denoted by the symbol $\backslash$). If $Y \neq X$, the link $X_{t-\tau} \to Y_t$ represents a *coupling at lag* τ, while for $Y = X$ it represents an *autodependency at lag* τ. Further, nodes X_t and Y_t are connected by an undirected contemporaneous link X_t—Y_t (Eichler 2012) if and only if

$$X_t \not\perp\!\!\!\perp Y_t \,|\, \mathbf{X}_{t+1}^- \backslash \{X_t, Y_t\}, \tag{4}$$

where also the contemporaneous present $\mathbf{X}_t \backslash \{X_t, Y_t\}$ is included in the condition. Note that stationarity implies that $X_{t-\tau} \to Y_t$ whenever $X_{t'-\tau} \to Y_{t'}$ for any t'.

While this definition applies to very general nonlinear interactions (Runge et al. 2012b), for a linear description, the conditional independencies can easily be related to the coefficients of a linear model. Model Eq. (1) can be written in matrix notation as

$$\begin{pmatrix} X_t \\ Y_t \end{pmatrix} = \underbrace{\begin{pmatrix} a & 0 \\ c & b \end{pmatrix}}_{\mathbf{\Phi}(1)} \begin{pmatrix} X_{t-1} \\ Y_{t-1} \end{pmatrix} + \begin{pmatrix} \varepsilon_t^X \\ \varepsilon_t^Y \end{pmatrix}, \tag{5}$$

where $\mathbf{\Phi}(1)$ is the lag-1 coefficient matrix and higher lags are null matrices: $\mathbf{\Phi}(s) = 0$ for $s > 1$. Now it can be shown that for models of this class [given by Eq. (B1) in appendix B] each coefficient in the matrix $\mathbf{\Phi}(1)$ corresponds to a directed link pointing forward in time and each nonzero value in the inverse covariance matrix $\mathbf{\Sigma}$ of the innovation ε corresponds to an undirected contemporaneous link (Eichler 2012).

It is important to note that these graphs can be linked to the concept of a lag-specific *Granger causality* (Granger 1969). Granger causality measures whether the prediction of one process is improved by taking into account another one. More precisely, in the original definition of Granger causality, $X \in \mathbf{X}$ Granger causes $Y \in \mathbf{X}$ with respect to the past of the whole process $\mathbf{X}$ if 1) events in X occur before events in Y and 2) X improves forecasting Y even if the past of the remaining process $\mathbf{X}\backslash\{X, Y\}$ is known. The latter property is directly related to the conditional dependence between X at some lag and Y given the past of the remaining process $\mathbf{X}\backslash\{X, Y\}$ that defines links in the time series graph.

The definition of the novel partial-correlation measure and the corresponding regression is based on the important notion of *parents* $\mathcal{P}_{Y_t}$ of a process Y_t in the time series graph. They are defined as

$$\mathcal{P}_{Y_t} \equiv \{Z_{t-\tau} : Z \in \mathbf{X}, \tau > 0, Z_{t-\tau} \to Y_t\}, \tag{6}$$

and the *neighbors* $\mathcal{N}_{Y_t}$ as

$$\mathcal{N}_{Y_t} \equiv \{X_t : X \in \mathbf{X}, X_t - Y_t\}. \tag{7}$$

Note that also the past lags of Y can be part of the parents. For example, in Fig. 7 the parents of Y_t are $\{Y_{t-1}, X_{t-1}\}$ and the only neighbor is X_t. The parents of all subprocesses in $\mathbf{X}$ together with the contemporaneous links comprise the time series graph.

b. Estimation

The time series graph can be estimated by different methods. In Runge et al. (2012b), a modification of the PC algorithm (Spirtes et al. 2001), named after its inventors Peter and Clark, for the estimation of the general nonlinear time series graphs using the information theoretic measure *conditional mutual information* (Cover and Thomas 2006) is described. Here, the focus lies on the linear case (as in the original introduction by Granger) and in the analyses of the following sections, the PC

algorithm in combination with *partial correlation* (as introduced in the next section) is used to measure conditional linear dependence.

Since the PC algorithm was originally introduced to estimate graphical models where no information about time order is assumed in the data, it consists of two steps: in the first step only undirected links are inferred, which are tested for directionality in the second step. This approach is also adopted in Ebert-Uphoff and Deng (2012a). But in our case of time series, the time ordering of nodes already provides the directionality and we omit the second step. Instead, we estimate the above-defined contemporaneous links without trying to assess a directionality. Note that due to a too large sampling time step of the data, a monthly contemporaneous link could actually be a lagged directional link on a daily time scale.

As an illustration of how the modified PC algorithm estimates the time series graph shown in Fig. 7 for model Eq. (1), consider the inference of the parents of Y_t. The algorithm tests possible links from all processes (including Y) at all lags up to a maximum delay. Here, the hypothetical link $X_{t-2} \to Y_t$ would be tested by first checking whether the ''unconditional'' cross correlation $\rho(X_{t-2}; Y_t)$ is nonzero. The graph-theoretical approach can explain that this is the case because there exists a path between X_{t-2} and Y_t (this path–theoretic interpretation is discussed in appendix B). In the next iteration step, the conditional linear dependence is tested. As a heuristic for selecting the conditions in each test, we choose the conditions sorted by their absolute correlation value in the previous step. In our example, the partial correlation $\rho(X_{t-2}; Y_t \,|\, Y_{t-1})$, which excludes the influence of Y_{t-1}, would be tested [because $|\rho(Y_{t-1}; Y_t)| > |\rho(X_{t-1}; Y_t)| > \ldots$]. This partial correlation would be nonzero due to the unblocked path $X_{t-2} \to X_{t-1} \to Y_t$. Also, the test with the next largest condition on X_{t-1} yields a nonzero partial correlation. After some more tests with ''weaker'' conditions, two conditions are used and the partial correlation $\rho(X_{t-2}; Y_t \,|\, Y_{t-1}, X_{t-1})$ would be found to vanish because all paths are blocked, such that the hypothetical link can be removed. If the iteratively increasing number of conditions equals the number of remaining parents and the partial correlation is still nonzero, a causal link has been found. In analogy, contemporaneous links are inferred by conditioning iteratively on more and more neighbors and additionally conditioning on all their parents (Runge et al. 2012b).

The free parameter of the algorithm is the maximum time lag to be considered. Some further parameters can be used to speed up the convergence and limit the computation time: for example, the initial and maximum number of conditions to take into account and the number of different conditions to test. How these parameters influence the convergence speed and other characteristics of the algorithm is further discussed in Runge et al. (2012b).

Different tests are possible for the null hypothesis that a link does not exist. For the information–theoretic quantities usually no theoretical results about the sampling distribution exists, and in Runge et al. (2012b) a shuffle test is proposed to at least approximate this distribution. The use of partial correlation, however, has the advantage that the sampling distribution is known and theoretical significance thresholds for different α levels can be used. Like Ebert-Uphoff and Deng (2012a), we also adopt this approach.

c. Discussion

It is important to note that the goal in the PC algorithm used in Ebert-Uphoff and Deng (2012a) is only to test for the *existence* of links but not to quantify their strength. In Ebert-Uphoff and Deng (2012a) links that are still present at higher significance levels are called *strong* while we prefer to use this term for the value of the partial-correlation measure introduced in the next section. The strength and level of significance of a link are two distinct properties. Strong links can vanish at low α levels and weak links can be highly significant. We refer to those highly significant links as more *robust* and check different α levels in our examples.

A problem we found with the significance test is that, for example, the distribution of $\hat{\rho}(X_{t-2}; Y_t \,|\, Y_{t-1})$ is still ''inflated'' by autocorrelations in X that is not accounted for in the theoretical alpha level. However, this is not the case for the novel partial-correlation measure. In appendix A, we further discuss general limitations and estimation issues of the time series graph inference algorithm.

6. Partial correlation and regression using time series graphs

The determination of the strength and delay of a mechanism now is a two-step procedure. In the first step the time series graph is estimated, which determines the existence or absence of a link and thus of a (Granger) causality between lagged components of $\mathbf{X}$. The coupling delay between $X \in \mathbf{X}$ and $Y \in \mathbf{X}$ is precisely defined by the nonzero link $X_{t-\tau} \to Y_t$ (or possibly more than one link at different lags τ) in the time series graph. In the second step discussed now, the *weight* of each assessed causal link is determined using the novel partial-correlation measure. Additionally, the determined parents and neighbors can be used in a multivariate regression.

Partial correlation measures the correlation between two variables with the influence of a set of controlling variables removed (partialed out). We explain it in the

framework of regression analysis, which in climate research is widely used for estimating the linear influence of possibly multiple variables, the *regressors* $\mathbf{U}$, on (the mean of) a *dependent* variable Y. If one regresses two variables X and Y on the same regressors $\mathbf{U}$, then the cross correlation between the residuals

$$\begin{aligned} X_{\mathbf{U}} &= X - \mathbf{U}\boldsymbol{\Gamma}_{\mathbf{U}}^{-1}\boldsymbol{\Gamma}_{\mathbf{U};X} \\ Y_{\mathbf{U}} &= Y - \mathbf{U}\underbrace{\boldsymbol{\Gamma}_{\mathbf{U}}^{-1}\boldsymbol{\Gamma}_{\mathbf{U};Y}}_{\substack{\text{regression}\\ \text{coefficient}\\ \text{(vector)}}} \end{aligned} \tag{8}$$

is the *partial correlation* $\rho_{YX|\mathbf{U}} = \rho(X_{\mathbf{U}};Y_{\mathbf{U}})$. Here, $\boldsymbol{\Gamma}_{\mathbf{U}}$ is the covariance matrix of the regressors and $\boldsymbol{\Gamma}_{\mathbf{U};Y}$ is the covariance vector of each regressor with Y, analogously for X.

We seek for a partial-correlation measure for the strength of a coupling mechanism between $X_{t-\tau}$ and Y_t that is independent of the internal dynamics of X and Y to overcome the discussed ambiguities of the cross correlation. The question now is which influence to partial out (i.e., on what to condition?). We will show that the crucial idea is to define a measure that quantifies how much the variability in X at the exact lag τ *directly* influences Y_t, irrespective of the pasts of $X_{t-\tau}$ and Y_t. This measure of coupling strength is based on the parents Y *and* the parents of X. In analogy to the general information–theoretic measure described in Runge et al. (2012a), we call it ρ^{MIT}, where MIT stands for *momentary information transfer*, which in the linear case should be understood as *momentary variance transfer*. It is defined as

$$\rho^{\mathrm{MIT}}_{X\to Y}(\tau) \equiv \rho(X_{t-\tau}; Y_t \,|\, \mathcal{P}_{Y_t}\backslash\{X_{t-\tau}\}, \mathcal{P}_{X_{t-\tau}}). \tag{9}$$

That is, MIT is the cross correlation of the residuals after $X_{t-\tau}$ and Y_t have been regressed on both the parents of $X_{t-\tau}$ and Y_t [i.e., the residuals in Eq. (8) for $\mathbf{U} = (\mathcal{P}_{Y_t}\backslash X_{t-\tau}, \mathcal{P}_{X_{t-\tau}})$]. The attribute *momentary* (Pompe and Runge 2011) is used because MIT measures the variance of the ''moment'' $t-\tau$ in X that is transferred to Y_t. One can also define a contemporaneous MIT, which in the linear case of an autoregressive model is equivalent to the normalized inverse covariance of the residuals after regressing each process on its parents (Runge et al. 2012a). For model Eq. (3), this corresponds to the inverse of the innovation's covariance matrix $\boldsymbol{\Sigma}$.

Importantly, MIT differs from the partial correlation used in the PC algorithm, named *information transfer to Y* (ITY) in Runge et al. (2012a), which only excludes the effect of the parents of Y, defined as

$$\rho^{\mathrm{ITY}}_{X\to Y}(\tau) \equiv \rho(X_{t-\tau}; Y_t \,|\, \mathcal{P}_{Y_t}\backslash\{X_{t-\tau}\}). \tag{10}$$

In analogy, for every variable $Y \in \mathbf{X}$ we define a (multivariate) MIT regression where the parents $\mathcal{P}_{Y_t}$ are taken as regressors $\mathbf{U}^{\mathrm{MIT}}_Y$. The residual's covariance and inverse covariance matrix can then be estimated from the regression residuals.

In the next section, we compare the different measures on climatological examples. For a detailed analytical comparison of the (partial) correlation measures for model example Eq. (1), further theoretical results and a description of bootstrap confidence bounds, we refer the interested reader to appendix B. In essence, the value of the cross correlation and also of the partial correlation ITY used in the PC algorithm depends on multiple coefficients and cannot be easily attributed to one single influence. On the contrary, one can prove that the MIT value solely depends on the underlying coupling parameter and the innovation's variances, that is, as shown in Table 2 the coefficient c and the variances σ_X^2, σ_Y^2 in model Eq. (1). MIT, thus, disentangles the correlation value and allows one to attribute the strength solely to the causal link, excluding the influence of other processes or autocorrelations. The strength of the autocorrelation can independently be quantified by the MIT of the autodependency links $[\rho^{\mathrm{MIT}}_{Y\to Y}(\tau)]$. Also a multivariate regression on the parents in the graph is easier to interpret because—as shown in Table 2—the regression recovers the coefficients of the model, without intermixing the coefficients as for the univariate regressions. A further practical advantage is that the MIT sampling distribution is not ''inflated'' by autocorrelation like that of cross correlation and ITY, allowing more accurate significance tests. In the next sections we show how these characteristics of MIT can be utilized to interpret climatological interactions.

7. Climatic examples

Now we analyze several bivariate climatic examples using the method developed in the previous sections to compare the different measures on real data. Further, we give a trivariate example to demonstrate that our approach can be used to detect more complicated interaction mechanisms. In addition to the surface air temperature indices Niño-3, ATL, WEUR, and EEUR analyzed in the motivating example in section 2, we study surface air temperatures in the eastern (EPAC) and central Pacific (CPAC) from the same dataset and monthly surface pressure anomalies over the western Pacific (WPAC), also from the National Centers for Environmental Prediction–National Center for Atmospheric Research (NCEP–NCAR) reanalysis (Kalnay et al.

1996) dataset. Further, the index SSA is the monthly precipitation rate anomaly over a region in southern South America (see map in Fig. 10) from the Global Precipitation Climatology Project (GPCP) dataset in years 1979–2012 (Adler et al. 2003). In all examples we run the algorithm with a maximum time lag of $\tau_{\max} = 15$ months and use a two-tailed significance level of $\alpha = 95\%$. More significance levels are also discussed at the end. Additionally, we show the 5% and 95% confidence bounds (i.e., the 90% confidence interval). The $\pm$ values given in the text roughly approximate the 90% confidence interval shown in the figures. Here, we focus on the statistical interpretation, while the results will be discussed climatologically in the next section.

a. Bivariate examples

In this section, we reexamine the European west–east link and the influences of Niño-3 on the tropical Atlantic and also on precipitation over southern South America. Further, we study the mutual interaction between the eastern and western Pacific.

The panels in Fig. 8 show the cross-correlation and autocorrelation lag functions in light gray. In the same plots we show the values of the PC algorithm measure ITY (dark gray) and MIT (black), where all nonsignificant links are marked by gray crosses. Contrary to the common plot of lag functions versus positive and negative lags τ shown in Fig. 1, the presentation as a matrix of lag functions with only nonnegative lags underlines the interpretation of the partial-correlation lag functions as directional influences in the sense of Granger causality. The estimated parents and neighbors of each variable can be read off from the ITY values in the columns in this matrix. First, we only compare MIT to the lagged cross correlation and discuss the more subtle differences between the PC algorithm measure ITY and MIT afterward.

Reexamining the motivating example of lag functions in the tropics and Europe, the strength of autocorrelation in Niño-3 as measured by MIT in Fig. 8b is very high and mostly coming from lags at $\tau = 1$ and 3, while lags farther in the past do not contribute much more for explaining the present. Also ATL has a strong autodependency MIT value at lag 1. In our model example analysis in section 3, such high autocorrelations resulted in a high and broad peak at a shifted lag in the cross-correlation function. Also here, most of the broad peak links in Niño-3 $\rightarrow$ ATL with a maximum at lag 4 are actually nonsignificant links. Rather, the MIT partial correlation is much smaller than the correlation and significant only at lag 1.

On the other hand, the peak at lag 1 for the cross-correlation WEUR $\rightarrow$ EEUR in Fig. 8b is not much reduced and the value $\rho^{\mathrm{MIT}} = 0.1 \pm 0.07$ even slightly larger than the link Niño-3 $\rightarrow$ ATL with $\rho^{\mathrm{MIT}} = 0.09 \pm 0.06$, albeit this difference is negligible considering the large confidence bounds. The European time series have almost no autocorrelation that could alter the position and value of the peak. Additionally, we performed a multivariate regression using $\mathbf{U}^{\mathrm{MIT}}$ with the parents inferred by the algorithm as regressors. The results are summarized in Table 3. Also here, we see that the coefficient of the multivariate regression of ATL on Niño-3 (1) is much smaller than that of the univariate regression shown in Table 1 at lag 4 (0.06 compared to 0.27), while the coefficients are unchanged in the European example within the error bounds. As can be seen from the R^2 values, Niño-3 and ATL are rather well explained by their regressors, while the variance in WEUR and EEUR comes almost entirely from the innovation's variance. In Figs. 8a and 8b the black solid lines are the numerically evaluated cross correlations for a multivariate autoregressive process with the same coefficients and innovations of Gaussian white noise with the same covariance matrix as the original residuals. The fitted lines well agree with the estimated correlations. This demonstrates that a large part of the covariance structure can be explained by a Gaussian model based on the time series graph.

While the MIT values of the Niño-3 $\rightarrow$ ATL and WEUR $\rightarrow$ EEUR links are equal within confidence bounds, the ITY value of Niño-3 $\rightarrow$ ATL is significantly larger than the corresponding MIT value (0.22 ± 0.06 compared to 0.09 ± 0.06). As discussed in the analytical comparison in appendix B, the reason is that ITY becomes larger for strong autocorrelations within X, here within Niño-3. A further difference is that some values that are significant for ITY became nonsignificant for MIT, for example, the autodependency link within Niño-3 at lag 5: again, the reason being that the sample distribution of the partial correlation ITY is inflated for strong autocorrelations.

These differences between the measure ITY used in the PC algorithm and MIT are further explored by the climatic examples in Figs. 8c and 8d. Figure 8c shows that the precipitation rate over South America (SSA) has no significant auto-ITY or auto-MIT value corresponding to a zero coefficient b in our model example Eq. (1) and we would not expect a shift of the peak of the cross-correlation function that is also not the case here. But the exclusion of autocorrelation in Niño-3 significantly reduces the value of MIT (0.19 ± 0.07) compared to ITY (0.29 ± 0.10) and the correlation (0.29 ± 0.08) of the link Niño-3 $\rightarrow$ SSA lag 1. In Fig. 8d we observe both cases in a feedback. The weakly autocorrelated WPAC drives (and is driven by) the highly autocorrelated

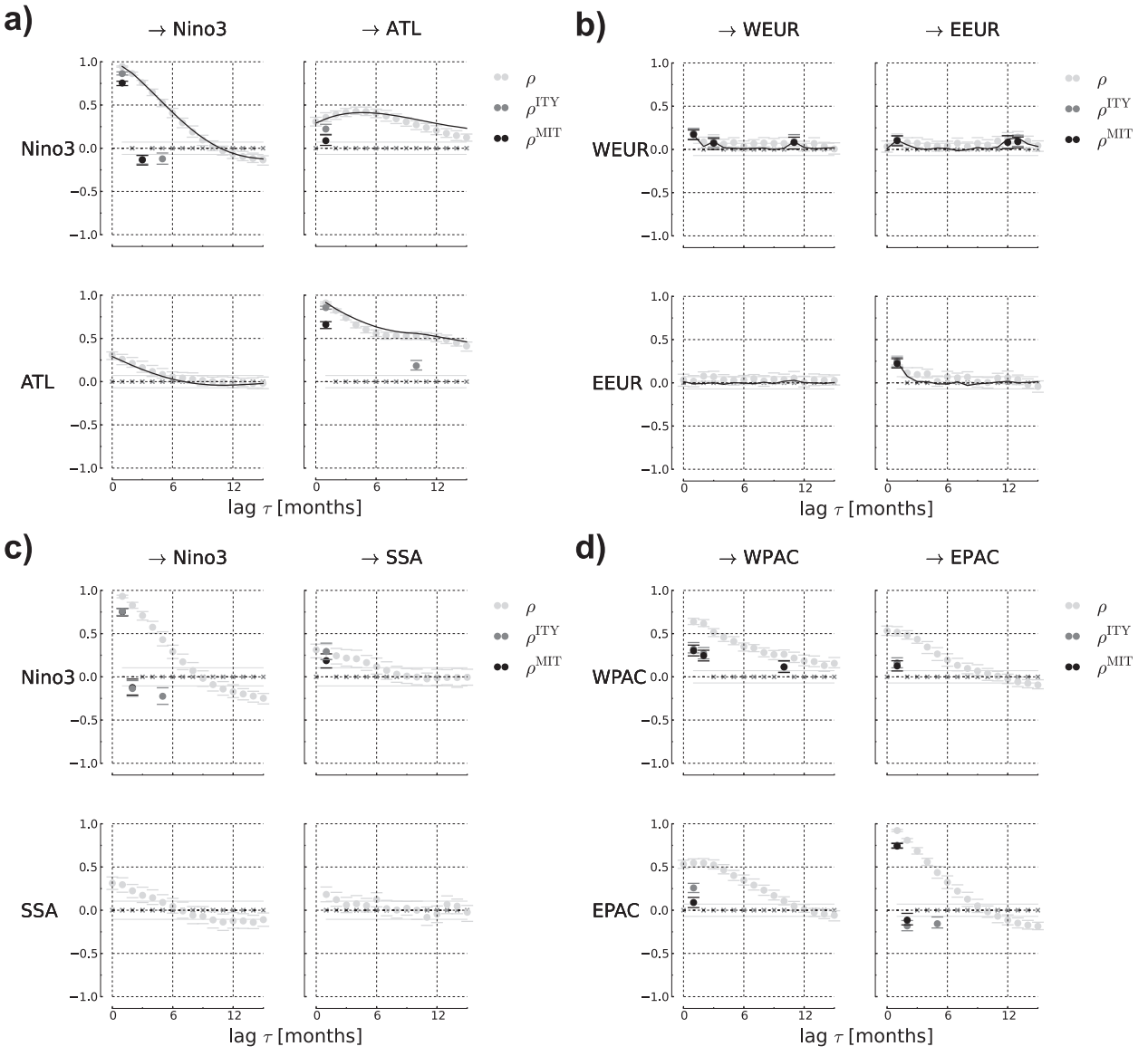

FIG. 8. Correlations and partial correlations of (a)–(d) four climatic example pairs. The matrix of lag functions in each panel shows the autocorrelations and correlations (light gray) and the values of ITY (dark gray) and MIT (black), where nonsignificant links are marked by gray crosses. The horizontal gray line denotes the two-sided 95% significance level (here without taking into account autocorrelation) for the correlations and autocorrelations. The error bars mark the 90% confidence interval. For example, (a) the upper right plot shows the lagged cross-correlation function $\rho(\text{Niño-3}_{t-\tau};\, \text{ATL}_t)$ for $\tau \geq 0$ in light gray and the ITY and MIT value at the only significant link $\text{Nino3}_{t-1} \to \text{ATL}_t$ in dark gray and black. For this link, MIT is the partial correlation $\rho(\text{Nino3}_{t-1}; \text{ATL}_t \,|\, \mathcal{P}_{\text{ATL}_t} \backslash \{\text{Nino3}_{t-1}\}, \mathcal{P}_{\text{Nino3}_{t-1}})$ with parents $\mathcal{P}_{\text{ATL}_t} \backslash \{\text{Nino3}_{t-1}\} = \{\text{ATL}_{t-1}, \text{ATL}_{t-10}\}$ and $\mathcal{P}_{\text{Nino3}_{t-1}} = \{\text{Nino3}_{t-2}, \text{Nino3}_{t-4}, \text{Nino3}_{t-6}\}$. Note that for autocorrelations (on the diagonal) the 0 lag is not drawn. (a),(b) The solid black lines mark the numerically evaluated cross correlations for a Gaussian model fitted to the time series according to Table 3. The plots demonstrate that much of the correlation links are actually merely due to the autocorrelation and show the differences between ITY and MIT.

EPAC at lag 1. The link WPAC → EPAC could have actually easily been overseen in a cross-correlation analysis because it is not at the peak of the lag function. While here the values of ITY and MIT are almost equal (0.13 ± 0.06 for MIT versus 0.16 ± 0.06 for ITY), for EPAC → WPAC the value of MIT is much smaller than that of ITY (0.09 ± 0.05 versus 0.26 ± 0.06). Note that ITY does *not* entirely exclude autocorrelation in Y as shown in Table 2. In Fig. C1a of appendix C, we also show a 30-yr sliding window analysis of this pair and note that the EPAC → WPAC link is observed more or less for the entire 1948–2012 period, while the

TABLE 3. Results of MIT (multivariate) regression analyses (after subtracting the mean) and the covariance matrix of the residuals. The parents of every dependent variable in the time series graph are chosen as regressors, which can be read off the columns in Figs. 8a and 8b. The coefficients of links relevant for the discussion are in bold.

Dependent Variable	Coef (lag τ)	Estimate	Std. error	p value
Niño-3	Niño-3 (1)	1.10	0.02	$<10^{-5}$
	Niño-3 (3)	−0.12	0.04	$<10^{-3}$
	Niño-3 (5)	−0.08	0.02	$<10^{-3}$
				$R^2 = 0.91$
ATL	ATL (1)	0.83	0.02	$<10^{-5}$
	ATL (10)	0.09	0.02	$<10^{-5}$
	Niño-3 (1)	**0.06**	0.01	$<10^{-5}$
				$R^2 = 0.84$
	Niño-3	ATL		
Niño-3	0.05	0.0004		
ATL		0.03		
WEUR	WEUR (1)	0.18	0.04	$<10^{-5}$
	WEUR (3)	0.08	0.04	≈0.03
	WEUR (11)	0.08	0.04	≈0.02
				$R^2 = 0.05$
EEUR	EEUR (1)	0.24	0.03	$<10^{-5}$
	WEUR (1)	**0.15**	0.05	≈0.004
	WEUR (12)	0.12	0.05	≈0.02
	WEUR (13)	0.14	0.05	≈0.01
				$R^2 = 0.10$
	WEUR	EEUR		
WEUR	2.11	−0.02		
EEUR		4.60		

WPAC → EPAC interaction becomes significant only from 1970 on.

Summarizing, we find a Niño-3 → ATL link with a delay of 1 month rather than the broad peak around 4 months in the cross correlation, while for the other examples without strong autocorrelations in both variables the lag is—as expected—not shifted, but only the value differs apart from the weakly autocorrelated European time series. We have tested the robustness of these examples by running the algorithm at different significance levels. As expected, the previously detected and more links occur for $\alpha < 95\%$ levels, at 97% the links Niño-3 → ATL and WPAC → EPAC vanish, at 99% also EPAC → WPAC vanishes, and at 99.9% also WEUR → EEUR becomes nonsignificant, while the strong Niño-3 → SSA is still significant.

b. Mechanism of the Walker circulation

In the previous example we have only considered the bivariate case, now the power of our approach will be demonstrated by taking into account another variable in the Pacific EPAC–WPAC example and constructing the time series graph for this three variable process.

To test whether the feedback between EPAC and WPAC was mediated via the surface of the central equatorial Pacific, we study the three variable process (EPAC, CPAC, and WPAC) where CPAC is a time series of the average surface air temperature over a region in the central Pacific shown on the map in Fig. 10 (5°S–5°N, 150°–120°W). Figure 9 shows the analysis using the same significance level as before. The parents inferred are $\mathcal{P}_{W_t} = \{W_{t-1}, W_{t-2}, W_{t-10}, W_{t-15}, C_{t-1}, E_{t-1}\}$, $\mathcal{P}_{C_t} = \{C_{t-1}, C_{t-3}, E_{t-1}, E_{t-7}\}$, and $\mathcal{P}_{E_t} = \{E_{t-1}, E_{t-2}, E_{t-5}, W_{t-1}\}$, where we abbreviated the variables by their first letter. Further, we found the contemporaneous links $E_t - C_t$ and $C_t - W_t$. Note that—as mentioned before—since the parents and neighbors are inferred with ITY, some of the corresponding links can have nonsignificant MIT values. The lagged cross correlation between EPAC and CPAC is broadly peaked around lag 1 with a peak value of 0.75 ± 0.04. The MIT values are 0.32 ± 0.05 for the contemporaneous link and 0.15 ± 0.07 for the link EPAC → CPAC at lag 1. It seems that the strong contemporaneous link prevents the peak from being shifted toward larger lags as would be expected for such strong autocorrelations. Note that the two links at lags 0 and 1 are an example of a side path discussed in appendix B, and the MIT value at lag 1, therefore, cannot be unambiguously related to this link. Further, CPAC drives WPAC with a lag 1. Very interestingly, the link EPAC → WPAC, which was robust before, vanishes. This result holds even for a low significance level of 95%. This link was obviously mediated via the surface of the equatorial central Pacific. On the other hand, the link back WPAC → EPAC does *not* vanish (only at higher significance levels), and the value is almost the same as in the bivariate example (0.14 ± 0.06). This shows that the link back takes a different path, not via the surface of the equatorial central Pacific. Also these results are recovered in a sliding window analysis as shown in Fig. C1b of appendix C. Interestingly, the MIT value of the link WPAC → EPAC along a distance of about 14 500 km is of the same strength as the CPAC → WPAC link with a distance of about 9500 km.

Summarizing this statistical perspective, for the bivariate examples we confirm the findings from our analytical model study and can explain the differences between cross correlation, ITY, and MIT. The trivariate example further demonstrates the power to detect indirect links not only in autodependencies (leading to shifted peaks) but also between multiple processes.

8. Climatological discussion

We now discuss the results of the previous section from a climatological perspective. All results are shown in Fig. 10 along with the regions used in the analysis.

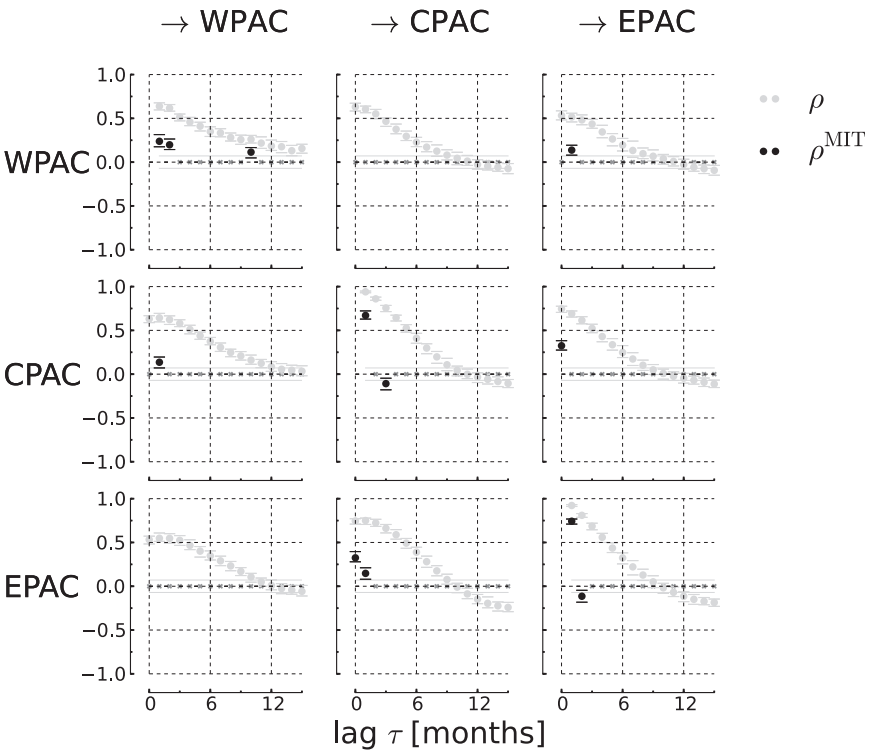

FIG. 9. Cross correlation (gray) and significant MIT values (black) for all pairs of variables (WPAC, CPAC, and EPAC). For example, here MIT for the link CPAC → WPAC is the partial correlation $\rho(C_{t-1}; W_t \,|\, \mathcal{P}_{W_t} \backslash \{C_{t-1}\}, \mathcal{P}_{C_{t-1}})$ with parents as given in the main text. The most important finding is the vanishing link EPAC → WPAC, which shows that the influence of the east on the west Pacific is mediated via the surface of the equatorial central Pacific. On the other hand the link WPAC → EPAC stays, implying that this influence was not mediated via this region.

For the European example, we have found almost no difference between the lagged cross correlation and MIT, as expected due to weak autodependencies (i.e., low persistency) in the single time series. We have uncovered maxima for the European example cross-correlation function at 1- and 12–13-month time lags. The 1-month time lag is in good agreement with the characteristic time scale $t_\star = L^2/4K$ for the turbulent heat exchange between two points at a distance L, with K as the characteristic value of the corresponding turbulent coefficient, in the considered case of the synoptic-scale turbulent heat exchange in the mid-latitudes with L about 3×10^6 m and K about 10^6-$\mathrm{m^2\,s^{-1}}$ (Stone and Yao 1987). This yields $t_\star$ about 2.4×10^6 s = 30 days. This estimation well corresponds to quasi-stationary atmospheric planetary Rossby waves, which mediate this macroturbulent synoptic-scale heat exchange between western and eastern Europe on the considered (monthly) time scale, with a pronounced seasonality inherent in these waves (Palmén and Newton 1969).

Also for the influence of Niño-3 on precipitation anomalies in southern South America, the peak of the cross correlation is at the same lag as the "causal" link inferred in the algorithm. But here the MIT value is smaller than the maximum of the cross correlation. This could be understood as an effect of the strong inertia in the tropical Pacific due to its large specific heat capacity. This implies that a large part of the covariation between Niño-3 and SSA is driven by a persistent momentum contribution from the past months in Niño-3 due to the large oceanic heat capacity. MIT attempts to exclude these internal dynamics by "conditioning out" information in the past of both processes, resulting in a smaller value than the cross correlation. Still, the MIT value is the strongest coupling mechanism among the four studied bivariate examples.

For the Pacific–Atlantic teleconnection we have found that a model with a link Niño-3 → ATL at lag 1 well explains the observed cross-correlation function, which peaks at lag 4. A lag of about 3–6 months is also reported in many other studies (e.g., Enfield and Mayer

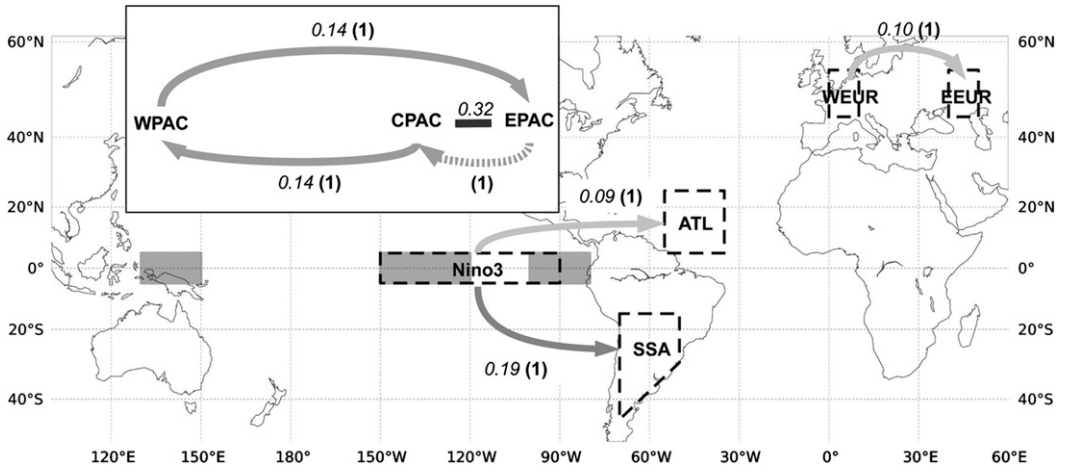

FIG. 10. Overview over important links determined in the analyses. The black dashed boxes denote the regions used in the bivariate analyses, while the gray boxes show the three regions analyzed to study the Walker circulation (see the inset). The arrows indicate the direction with the gray shading roughly corresponding to the MIT strength. The undirected line CPAC—EPAC denotes the contemporaneous link and the link EPAC → CPAC is drawn dashed because this link has a side path via the contemporaneous link and the MIT can, therefore, not unambiguously be attributed to this link. The label gives the MIT value and time lag in months in parentheses. Note that the 5% and 95% confidence bounds of these MIT values are typically ±0.06.

1997; Giannini et al. 2000; Wang and Enfield 2006; Chang et al. 2006). These studies also report higher peak values than we measure for the MIT. How can this difference be explained? What lags do the two approaches measure? In section 4, we have given the simple picture of a particle Y fluctuating in a shallow potential well that models the internal dynamics. This particle is subject to random forces and to the external system X that acts on Y with a certain coupling delay τ via a coupling mechanism. In the Pacific–Atlantic teleconnection, this coupling mechanism corresponds to the ''heat signal'' being advected from Niño-3 to the Atlantic region's atmospheric column by the Pacific–Atlantic Walker circulation. The characteristic horizontal velocity V of this process is about 1–2 m s^{-1} (Wang 2002), which well explains the delay of $\tau = L_{\mathrm{NA}}/V = 1$ month estimated in the time series graph for this distance $L_{\mathrm{NA}} = 8.3 \times 10^6$ m. After the signal arrived, the strong internal dynamics of the Atlantic in the oceanic mixed layer (OML) underlying the surface air counteract these perturbations. Any initial increase or decrease in surface air temperature forces an immediate reaction of the opposite sign in the sensible and latent heat fluxes to the atmosphere from the OML—with a thickness of about 20–30 m in the equatorial regions—and the latter begins to cool or warm with a characteristic time scale of about 3–6 months. This process is accompanied by the corresponding changes in the surface winds and the lower atmosphere vertical velocities. We believe that this is the time delay quantified by the cross correlation, which measures the aggregate effect of the coupling mechanism plus internal dynamics. Apart from the coupling delay, we have found that the MIT values of the Pacific–Atlantic teleconnection and the European teleconnection were the same, suggesting that the coupling mechanisms via the Pacific–Atlantic Walker circulation and the synoptic macroturbulence and planetary Rossby waves are actually of the same strength, while the physics is very different. Note also that the Atlantic and Pacific regions are much farther apart.

Last, concerning the EPAC → CPAC → WPAC → EPAC feedback loop (summarized in the inset in Fig. 10), the basic mechanism of the Walker circulation (Walker 1923, 1924; Bjerknes 1969; Rowntree 1972; Webster 1981; Wang 2002; Hosking 2012) suggests this circulation is primarily driven by heating on the western flanks of the equatorial oceans. The inset in Fig. 10, which is drawn on the basis of our results depicted in Fig. 9, illustrates well this feature for the Pacific branch of the above circulation. In normal and La Niña phases of ENSO, the latter is driven by strong sensible heating and latent heat release associated with penetrating moist convection in the western Pacific under a pronounced supply of the lower troposphere moisture there. The lower part of this circulation (see the inset in Fig. 10) promotes upwelling of waters in the eastern part of the Pacific Ocean and downwelling of waters in the western part. As far as oceanic temperatures decrease with increased depth, any decrease (increase) of surface pressure in the western part of the Pacific Ocean, which accompanies an increase (decrease) in sea and air surface temperatures and moist convection there, favors

a decrease (increase) of sea and air surface temperatures in the eastern and central Pacific. Our results track well this feature of the Pacific atmospheric and oceanic circulation: we have obtained a positive MIT value (like the cross correlation) between surface pressure over WPAC and surface air temperatures over EPAC.

The described above Walker circulation pattern over the Pacific Ocean is different during El Niño events, where the region of atmospheric updrafts shifts toward the central Pacific and also broadens out. A statistical analysis of the Walker circulation thus actually demands to investigate the different seasons (El Niño, La Niña, and normal conditions) separately. This will be studied in a forthcoming article; here, we used the whole time sample to test the hypothesis that the average influence is mediated via the central Pacific.

In summary, physically MIT is well interpretable as a measure that solely depends on the strength of a coupling mechanism and ''filters out'' internal dynamics (i.e., inertia or persistence) and even possible effects of external processes (if taken into account in the conditions). The strength of internal dynamics can be quantified by the corresponding auto-MIT value. The cross correlation, on the other hand, cannot separate these influences. Both approaches measure different aspects of an interaction, but we believe that the improved interpretability of MIT is better suited to assist in understanding the underlying physics.

9. Conclusions and outlook

Cross-correlation lag functions and regressions are commonly used to identify interaction mechanisms between climatological processes, in particular to assess possible time delays of a mechanism and as a measure to quantify the strength of the link mediated by the mechanism. In this article, we have investigated how justified such an approach is in the presence of large autocorrelations that typically occur in tropical temperature time series. An analytical study of a simple autoregressive model suggests that univariate regression coefficients and the cross-correlation lag function's maximum value and lag are very sensitive to even slight changes in high autocorrelation. Using the picture of a particle in a shallow potential we also give a physical explanation for this effect and come to the conclusion that cross-correlation and univariate regressions are quite ambiguously influenced by internal dynamics with strong inertia (e.g., a large oceanic heat capacity) and misguide an estimate of a physical coupling strength.

To overcome these issues, we propose a two-step procedure based on the concept of graphical models that has recently been introduced to climate research. In a first step, graphical models are used to detect the existence of (Granger) causal interactions yielding the time delay of the coupling mechanism, while in a second step a certain partial correlation and a regression measure, based on the idea of momentary information transfer (MIT), are introduced that allow one to specifically quantify the strength of an interaction mechanism. This enables us to exclude misleading effects of serial correlation as well as more general dependencies, a feature that can also be proven for very general processes and makes MIT well interpretable.

Our method is then applied to several climatic examples. For the influence of the tropical east Pacific on the northern tropical Atlantic, we detect a short lag of 1 month for this coupling mechanism consistent with the advection speed of the Pacific–Atlantic Walker circulation, while previous studies using the maximum of the cross-correlation lag function found lags of 3–6 months. Also, we uncover that the coupling mechanism is actually quite weak (even comparable to the coupling mechanism between western and eastern Europe) and that the large cross-correlation value can be explained by strong autocorrelations present in both time series.

As a further step, the potential of our approach to quantify the interactions also between more than two variables is demonstrated by investigating the mechanism of the Walker circulation. The purely statistical analysis confirms that the positive correlation of surface temperatures over the eastern Pacific and surface pressure over the western Pacific is mediated via the central Pacific while the lagged correlation back cannot be explained by variabilities in surface temperatures of the central Pacific. The time lags of this circulation are weeks to 1 month between the eastern and central Pacific, another month for the impact of the central Pacific on the western Pacific, and 1 month for the link back via the upper atmosphere. For the path CPAC $\rightarrow$ WPAC $\rightarrow$ EPAC, we find that the strength of these two mechanisms is very similar; even so, they act on very different distances.

Several questions remain to be investigated: in particular, why there seems to be no statistically significant link from the western Pacific to the central Pacific, although descent occurs along the whole equatorial Pacific (Hosking 2012). This question could be related to the point that the different phases of the Walker mechanism were not taken into account here. The modification of the presented method for this case will be studied in a forthcoming article.

In Runge et al. (2012a), we compare more alternative quantifications of coupling strength for the more general nonlinear case, also the information–theoretic analog to

Granger causality, *transfer entropy* (Schreiber 2000), and show that this measure also depends on autocorrelations.

Online (at http://tocsy.pik-potsdam.de/tigramite.php) we provide a program with a graphical user interface to estimate the time series graph and the partial correlation measures ITY and MIT and to create the figures shown in this article.

The approach introduced in this article aims at enabling climate researchers to statistically test specific hypotheses on interactions in the data. While the concept introduced here is purely statistical, it may serve as a first step to construct conceptual or more complex models of physical processes.

Acknowledgments. We appreciate the support by the German National Academic Foundation and the DFG Grant KU34-1. NCEP Reanalysis and GPCP data were provided by the NOAA/PSD, Boulder, Colorado (from their website at http://www.esrl.noaa.gov/psd/). Mathematica (http://www.wolfram.com/mathematica/) was used to generate the plots for the analytical model.

APPENDIX A

Further Remarks on Time Series Graph Estimation

As further discussed in Ebert-Uphoff and Deng (2012a), two main assumptions are underlying a causal inference with the PC algorithm. The first one is *faithfulness*, which guarantees that the graph entails all conditional independence relations true for the underlying process. Second, to call the links in the graph causal one assumes *causal sufficiency*, implying that no hidden common drivers are present. This assumption is obviously violated if a finite set of climatic variables is analyzed (given the continuous nature of physical processes) and we, therefore, would call these links only "(Granger) causal with respect to the variables taken into account."

Regarding estimation, one concern with the PC algorithm is the problem of sequential testing. That is, if each link is tested multiple times at the same α level, the resulting combined alpha level is higher, which should be kept in mind when interpreting the false positive rate of inferred links. This problem is usually treated by correcting for the number of tests (e.g., using a Bonferroni correction), but this number is not known a priori in the algorithm. Especially in the linear framework, an alternative to the PC algorithm is the direct fit of a specific model. Then one can control the false discovery rate (Benjamini and Hochberg 1995) with the drawback that the model might be incorrectly specified and more parameters need to be selected.

APPENDIX B

Analytical Comparison and General Theoretical Results

In this appendix, we give a detailed analytical comparison of the (partial) correlation measures for model example Eq. (1), further theoretical results, and discuss significance and confidence tests.

a. Derivation of covariances for model Eq. (1)

Here, we derive the analytical expressions for the covariances needed to evaluate the regressions, cross correlation, and the partial correlations ITY and MIT shown in Table 2. These results are discussed in section 2.

The model Eq. (1), here better discussed in the form of Eq. (5), belongs to the general class of vector autoregressive processes of order p defined as

$$\mathbf{X}_t = \sum_{s=1}^{p} \mathbf{\Phi}(s)\mathbf{X}_{t-s} + \boldsymbol{\varepsilon}_t, \tag{B1}$$

where $\mathbf{\Phi}(s)$ are the $M \times M$ matrices of coefficients for each lag s and the M-vector $\boldsymbol{\varepsilon}_t \sim \mathcal{N}(0, \mathbf{\Sigma})$ is an independent identically distributed Gaussian random variable with zero mean and covariance matrix $\mathbf{\Sigma}$. The random variable $\boldsymbol{\varepsilon}$ is sometimes referred to as the *innovation term.* Its variances on the main diagonal of $\mathbf{\Sigma}$ are denoted by σ_i^2 and the covariances by σ_{ij}.

For this model, there exists an analytical expression of the covariance in terms of $\mathbf{\Phi}$ (Brockwell and Davis 2009, chapter 11.3):

$$\mathbf{\Gamma}_{ij}(\tau) \equiv E(\mathbf{X}_{t+\tau}^i \mathbf{X}_t^j) = \sum_{n=0}^{\infty} [\mathbf{\Psi}(n+\tau)\mathbf{\Sigma}\mathbf{\Psi}^{\mathrm{T}}(n)]_{ij}, \tag{B2}$$

where the matrix $\mathbf{\Psi}(n)$ can be recursively computed from matrix products:

$$\mathbf{\Psi}(n) = \sum_{s=1}^{n} \mathbf{\Phi}(s)\mathbf{\Psi}(n-s). \tag{B3}$$

In the case of an AR(1) model, all coefficient matrices $\mathbf{\Phi}(s)$ with lags $s > 1$ are 0, and as can be seen from Eq. (B3), $\mathbf{\Psi}$ is simply given by the matrix powers of $\mathbf{\Phi}(1)$ that are

$$\mathbf{\Psi}(n) = \mathbf{\Phi}(1)^n = \begin{pmatrix} a & 0 \\ c & b \end{pmatrix}^n = \begin{bmatrix} a^n & 0 \\ (a^n - b^n)\dfrac{c}{a-b} & b^n \end{bmatrix}. \tag{B4}$$

Then the variances for $\tau = 0$ are

$$\Gamma_X = \sum_{n=0}^{\infty} [\mathbf{\Psi}(n)\mathbf{\Sigma}\mathbf{\Psi}^{\mathrm{T}}(n)]_{XX} = \sigma_X^2 \sum_{n=0}^{\infty} a^{2n} \tag{B5}$$

and

$$\Gamma_Y = \sum_{n=0}^{\infty} \{[\mathbf{\Psi}(n)\mathbf{\Sigma}\mathbf{\Psi}^{\mathrm{T}}(n)]\}_{YY} = \sum_{n=0}^{\infty} \left\{ \begin{array}{l} [(a-b)^2\sigma_Y^2 + c(c\sigma_X^2 - 2a\sigma_{XY} + 2b\sigma_{XY})]b^{2n} \\ +a^{2n}c^2\sigma_X^2 - 2a^n c(c\sigma_X^2 - a\sigma_{XY} + b\sigma_{XY})b^n \end{array} \right\}. \tag{B6}$$

Noting that the infinite sums are geometric series that converge assuming $0 < |a|, |b| < 1$, one arrives at the variances in Table 2 (where additionally σ_{XY} was set to 0). Similarly, the covariance function for the direction $Y \to X$ (valid for $\tau \leq 0$) is

$$\Gamma_{XY}(\tau) = \sum_{n=0}^{\infty} [\mathbf{\Psi}(n+\tau)\mathbf{\Sigma}\mathbf{\Psi}^{\mathrm{T}}(n)]_{XY} = \frac{1}{a-b} \sum_{n=0}^{\infty} a^{n+\tau}[a^n c\sigma_X^2 - b^n(c\sigma_X^2 - a\sigma_{XY} + b\sigma_{XY})], \tag{B7}$$

and for the direction $X \to Y$ (valid for $\tau > 0$) is

$$\Gamma_{YX}(\tau) = \sum_{n=0}^{\infty} [\mathbf{\Psi}(n+\tau)\mathbf{\Sigma}\mathbf{\Psi}^{\mathrm{T}}(n)]_{YX} = \frac{1}{a-b} \sum_{n=0}^{\infty} a^{n}[a^{n+\tau} c\sigma_X^2 - b^{n+\tau}(c\sigma_X^2 - a\sigma_{XY} + b\sigma_{XY})], \tag{B8}$$

from which the cross correlation in Table 2 follows (with $\sigma_{XY} = 0$). Note that $\Gamma_{YX}(\tau)$ does not diverge for $a = b$ since in this limit according to L'Hôpital's rule

$$\Gamma_{YX}(\tau) \overset{a=b}{=} \frac{b^{\tau-1}[bd(1-b^2) - b^2cs^2(\tau-1) + cs^2\tau]}{(1-b^2)^2}. \tag{B9}$$

As a check, for no autocorrelation, that is, for $a = b = 0$ and at the correct coupling lag $\tau = 1$, this gives

$$\Gamma_{YX}(1) \overset{a=b=0}{=} c\sigma_X^2. \tag{B10}$$

The inequality relation in the caption of Fig. 2 for zero contemporaneous dependency $\sigma_{XY} = 0$ is obtained from simplifying $\Gamma_{YX}(2) > \Gamma_{YX}(1)$ using the assumption that a and b are positive and smaller than 1. The regression coefficients are gained by inserting the previously derived covariances into the regression formula in Eq. (8). ITY can be derived by analogously computing $\Gamma_{YY}(1)$ and using the fact that the partial correlation $\rho(X_{t-1}; Y_t \,|\, Y_{t-1})$ is equivalent to the cross correlation of the residuals of X_{t-1} and Y_t after regression on Y_{t-1}. This leads to the residual covariance $\Gamma_{YX}(1) - \Gamma_{YX}(0)\Gamma_{YY}(1)/\Gamma_Y$ and the residual variances $\Gamma_Y - \Gamma_{YY}(1)^2\Gamma_Y$ and $\Gamma_X - \Gamma_{YX}(0)^2\Gamma_Y$ from which the value in Table 2 follows (with $\sigma_{XY} = 0$). MIT could be similarly computed but also follows from the coupling strength autonomy theorem [Eq. (B12)].

b. *Analytical comparison and general theoretical results*

We now discuss the differences between univariate and MIT regressions and compare cross correlation and the partial correlations ITY (used in the PC algorithm) and MIT for the model example Eq. (1) with no contemporaneous dependence, $\sigma_{XY} = 0$.

First, we give a brief graph–theoretic analysis of the cross-correlation function of model Eq. (1) to further illustrate its dependencies. The lagged covariance Eq. (B2) can be expressed as

$$\Gamma_{YX}(\tau) = \sum_{n=0}^{\infty} [\mathbf{\Phi}(1)^{n+\tau}\Sigma\mathbf{\Phi}(1)^{n^{\mathrm{T}}}]_{YX}. \tag{B11}$$

Graph–theoretically, a nonzero coefficient $[\mathbf{\Phi}(1)^3]_{YX} \neq 0$ corresponds to the number of paths composed of three links, each with lag 1, for example, $X_{t-3} \to X_{t-2} \to Y_{t-1} \to Y_t$. The covariance $\Gamma_{YX}(\tau)$ then is an infinite sum of the triple product of matrix powers composed of the coefficient and innovation's covariance matrix and therefore a nonlinear polynomial combination of coefficients of *all possible paths* that end in X and τ lags later in Y, emanating from nodes and their neighbors (*contemporaneous* nodes at the same time lag) at all possible lags. These paths can be nicely read off from the time series graph as in Fig. 7. In essence, most spurious links in the cross-correlation lag function are due to the common driver effect of past lags (Fig. 6b) or the indirect causal effect due to intermediate lags (Fig. 6a).

In Table 2, the dependence of the cross correlation and regressions on the model parameters is given as plotted in Figs. 2 and 4. As opposed to these complicated dependencies, those of the partial-correlation measures are much simpler. First, ITY and MIT are nonzero only at the causal time lag $\tau = 1$. Regarding the value, we find that—counterintuitively—ITY actually still depends on the autocorrelation strength parameter b for this model,

even so the past lag of Y is used as a condition. Only MIT fully excludes both influences.

This result can be even more generalized in that for a link $X_{t-\tau} \to Y_t$ in a general linear vector autoregressive processes [given by model Eq. (B1)], MIT can be shown to generally depend solely on the corresponding coupling coefficient in $\Phi_{YX}(\tau)$ and the variances σ_X^2, σ_Y^2 in the innovation's covariance matrix $\mathbf{\Sigma}$:

$$\rho^{\mathrm{MIT}}_{X\to Y}(\tau) = \frac{\Phi_{YX}(\tau)\sigma_X}{\sqrt{[\Phi_{YX}(\tau)]^2\sigma_X^2+\sigma_Y^2}}. \qquad \text{(B12)}$$

This formula is the linear version of the *coupling strength autonomy theorem* that treats the general nonlinear case (Runge et al. 2012a). One case, where the influence of X at lag $t-\tau$ cannot be unambiguously related to the link $X_{t-\tau} \to Y_t$ alone is shown in Fig. 7 for $\tau = 1$, where another path of influence is $X_{t-\tau} - Y_{t-1} \to Y_t$, which vanishes for $\sigma_{XY} = 0$. These side paths are further discussed in Runge et al. (2012a), where we also proved that the value of MIT is always smaller or equal to ITY.

Also a multivariate regression on the parents in the graph is easier to interpret, because—as shown in Table 2—the regression recovers the coefficients of the model, without intermixing the coefficients as for the univariate regressions. In analogy to the coupling strength autonomy theorem, for the regressions a similar theorem holds in that also for a general multivariate autoregressive process given by Eq. (B1), $\mathbf{U}_Y^{\mathrm{MIT}}$ can be shown to yield the corresponding coefficients in the lagged matrices $\mathbf{\Phi}(s)$. Regression coefficients for the regression on $\mathbf{U}_Y^{\mathrm{MIT}}$ and the partial-correlation measure MIT capture different aspects of a coupling mechanism. A regression coefficient of a parent $X_{t-\tau}$ gives the scale factor that determines the proportion of $X_{t-\tau}$ influencing Y_t. The partial correlation, on the other hand, is a *normalized* measure and can, thus, be better compared to the partial correlation of other processes with quite different innovation's variances.

c. *Remark on significance testing and confidence bounds*

The advantage of MIT to filter out autocorrelation can also be used for further significance testing because the sample coefficient $\widehat{\rho^{\mathrm{MIT}}_{X\to Y}}$ is not inflated by autocorrelation like the sample cross correlation and also the partial correlation ITY used in the PC algorithm. The MIT value of links inferred by the modified PC algorithm can, thus, become nonsignificant. Apart from significance testing, in the analyses of section 7 we also provide bootstrap confidence bounds (Efron and Tibshirani 1994) that allow one to quantify the uncertainty in the sample.

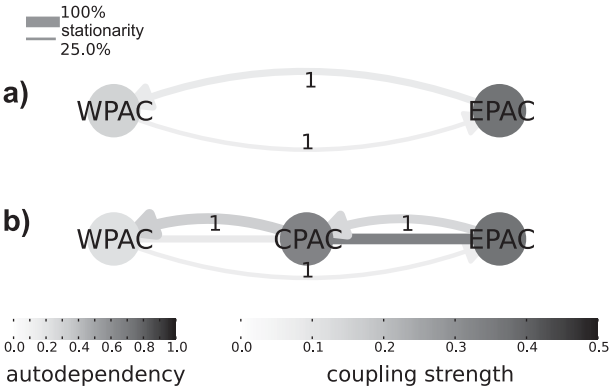

FIG. C1. Ensemble statistics of sliding window analysis of the bi- and trivariate Walker circulation examples. This kind of graph has been termed *process graph* in Runge et al. (2012b) that aggregates the information in the time series graph. The node shade denotes the ensemble average auto-MIT lag-1 strength and the link shade encodes the ensemble average MIT strength at the lag denoted in the link label. The link width, on the other hand, is proportional to the fraction of sliding windows with this link being significant.

These are computed from surrogates by drawing samples with replacement from the jointly lagged sample. For example, a surrogate for the partial correlation estimate $\hat{\rho}(X_{t-1}; Y_t \,|\, Y_{t-1})$ for a sample length of T is created by randomly choosing T triples of lagged samples (X_{t-1}, Y_t, Y_{t-1}) and estimating their partial correlation.

APPENDIX C

Further Stationarity Analysis of Walker Example

To further assess the stationarity of the Walker circulation example, we conducted a sliding window analysis with windows of length 30 yr (360 month samples) in steps of 3 yr leading to 12 windows (albeit only two are nonoverlapping). We used the same algorithm parameters and significance level as before. The results are shown in Fig. C1. As discussed in the main text, the link WPAC $\to$ EPAC is significant only after 1970 but unchanged in the bivariate (Fig. C1a) and trivariate (Fig. C1b) analyses. Apart from the contemporaneous link between CPAC and WPAC, all other links are rather stationary. Note that the use of daily data would yield more precise lags but also bring about the problem that a much larger number of significance tests has to be conducted.

REFERENCES

Adler, R. F., and Coauthors, 2003: The version 2 Global Precipitation Climatology Project (GPCP) monthly precipitation analysis (1979–present). *J. Hydrometeor.,* **4,** 1147–1167.

Benjamini, Y., and Y. Hochberg, 1995: Controlling the false discovery rate: A practical and powerful approach to multiple testing. *J. Roy. Stat. Soc.,* **57B,** 289–300.

Bjerknes, J., 1969: Atmospheric teleconnections from the equatorial Pacific. *Mon. Wea. Rev.,* **97,** 163–172.

Brockwell, P., and R. Davis, 2009: *Time Series: Theory and Methods.* 2nd ed. Springer, 579 pp.

Chang, P., Y. Fang, R. Saravanan, L. Ji, and H. Seidel, 2006: The cause of the fragile relationship between the Pacific El Niño and the Atlantic Niño. *Nature,* **443,** 324–328.

Chatfield, C., 2003: *The Analysis of Time Series: An Introduction.* Chapman and Hall/CRC, 352 pp.

Cover, T., and J. Thomas, 2006: *Elements of Information Theory.* 2nd ed. John Wiley and Sons, 776 pp.

Dahlhaus, R., 2000: Graphical interaction models for multivariate time series. *Metrika,* **51,** 157–172.

Ebert-Uphoff, I., and Y. Deng, 2012a: Causal discovery for climate research using graphical models. *J. Climate,* **25,** 5648–5665.

——, and ——, 2012b: A new type of climate network based on probabilistic graphical models: Results of boreal winter versus summer. *Geophys. Res. Lett.,* **39,** L19701, doi:10.1029/2012GL053269.

Ebisuzaki, W., 1997: A method to estimate the statistical significance of a correlation when the data are serially correlated. *J. Climate,* **10,** 2147–2153.

Efron, B., and R. Tibshirani, 1994: *An Introduction to the Bootstrap.* Chapman and Hall, 456 pp.

Eichler, M., 2005: A graphical approach for evaluating effective connectivity in neural systems. *Philos. Trans. Roy. Soc. London,* **B360,** 953–967.

——, 2012: Graphical modelling of multivariate time series. *Probab. Theory Relat. Fields,* **153,** 233–268.

Enfield, D. B., and A. Mayer, 1997: Tropical Atlantic sea surface temperature variability relation. *J. Geophys. Res.,* **102** (C1), 929–945.

Giannini, A., Y. Kushnir, and M. A. Cane, 2000: Interannual variability of Caribbean rainfall, ENSO, and the Atlantic Ocean. *J. Climate,* **13,** 297–311.

Granger, C. C., 1969: Investigating causal relations by econometric models and cross-spectral methods. *Econometrica,* **37,** 424–438.

Gu, G., and R. F. Adler, 2011: Precipitation and temperature variations on the interannual time scale: Assessing the impact of ENSO and volcanic eruptions. *J. Climate,* **24,** 2258–2270.

Hashizume, M., T. Terao, and N. Minakawa, 2009: The Indian Ocean dipole and malaria risk in the highlands of western Kenya. *Proc. Natl. Acad. Sci. USA,* **106,** 1857–1862.

Hosking, J., 2012: Tropical convective transport and the Walker circulation. *Atmos. Chem. Phys. Discuss.,* **12,** 12 229–12 244.

Huang, F., S. Zhou, S. Zhang, H. Wang, and L. Tang, 2011: Temporal correlation analysis between malaria and meteorological factors in Motuo County, Tibet. *Malar. J.,* **10** (54), doi:10.1186/1475-2875-10-54.

Kalnay, E., and Coauthors, 1996: The NCEP/NCAR 40-Year Reanalysis Project. *Bull. Amer. Meteor. Soc.,* **77,** 437–471.

Klein, S., B. Soden, and N. Lau, 1999: Remote sea surface temperature variations during ENSO: Evidence for a tropical atmospheric bridge. *J. Climate,* **12,** 917–932.

Lanzante, J., 1996: Lag relationships involving tropical sea surface temperatures. *J. Climate,* **9,** 2568–2578.

Lauritzen, S. L., 1996: *Graphical Models.* Oxford Statistical Science Series, Vol. 16, Clarendon Press, 308 pp.

Palmén, E., and C. W. Newton, 1969: *Atmospheric Circulation Systems: Their Structure and Physical Interpretation.* 13th ed. Academic Press, 603 pp.

Pompe, B., and J. Runge, 2011: Momentary information transfer as a coupling measure of time series. *Phys. Rev.,* **83E,** 051122, doi:10.1103/PhysRevE.83.051122.

Rodionov, S. N., 2006: Use of prewhitening in climate regime shift detection. *Geophys. Res. Lett.,* **33,** L12707, doi:10.1029/2006GL025904.

Rowntree, P., 1972: The influence of tropical east Pacific Ocean temperatures on the atmosphere. *Quart. J. Roy. Meteor. Soc.,* **98,** 290–321.

Runge, J., J. Heitzig, N. Marwan, and J. Kurths, 2012a: Quantifying causal coupling strength: A lag-specific measure for multivariate time series related to transfer entropy. *Phys. Rev.,* **86E,** 061121, doi:10.1103/PhysRevE.86.061121.

——, ——, V. Petoukhov, and J. Kurths, 2012b: Escaping the curse of dimensionality in estimating multivariate transfer entropy. *Phys. Rev. Lett.,* **108,** 258701, doi:10.1103/PhysRevLett.108.258701.

Schelter, B., M. Winterhalder, R. Dahlhaus, J. Kurths, and J. Timmer, 2006: Partial phase synchronization for multivariate synchronizing systems. *Phys. Rev. Lett.,* **96,** 208103, doi:10.1103/PhysRevLett.96.208103.

Schreiber, T., 2000: Measuring information transfer. *Phys. Rev. Lett.,* **85,** 461–464.

Spirtes, P., C. Glymour, and R. Scheines, 2001: *Causation, Prediction, and Search.* Adaptive Computation and Machine Learning Series, Vol. 81, MIT Press, 565 pp.

Stone, P. H., and M.-S. Yao, 1987: Development of a two-dimensional zonally averaged statistical–dynamical model. Part II: The role of eddy momentum fluxes in the general circulation and their parameterization. *J. Atmos. Sci.,* **44,** 3769–3786.

Von Storch, H., and F. Zwiers, 2002: *Statistical Analysis in Climate Research.* Cambridge University Press, 496 pp.

Walker, G. T., 1923: Correlation in seasonal variations of weather, VIII: A preliminary study of world weather. *Mem. Indian Meteor. Dep.,* **24** (4), 75–131.

——, 1924: Correlation in seasonal variations of weather, IX: A further study of world weather. *Mem. Indian Meteor. Dep.,* **24** (9), 275–332.

Wang, C., 2002: Atmospheric circulation cells associated with the El Niño–Southern Oscillation. *J. Climate,* **15,** 399–419.

——, and D. B. Enfield, 2006: Influences of the Atlantic warm pool on Western Hemisphere summer rainfall and Atlantic hurricanes. *J. Climate,* **19,** 3011–3028.

Wang, X. L., 2008: Accounting for autocorrelation in detecting mean shifts in climate data series using the penalized maximal *t* or *F* Test. *J. Appl. Meteor. Climatol.,* **47,** 2423–2444.

Webster, P., 1981: Mechanisms determining the atmospheric response to sea surface temperature anomalies. *J. Atmos. Sci.,* **38,** 554–571.

Zhang, X., 2004: Comment on ''Applicability of prewhitening to eliminate the influence of serial correlation on the Mann-Kendall test'' by Sheng Yue and Chun Yuan Wang. *Water Resour. Res.,* **40,** W03805, doi:10.1029/2003WR002073.

Zwiers, F. W., 1990: The effect of serial correlation on statistical inferences made with resampling procedures. *J. Climate,* **3,** 1452–1461.